Computational and Structural Biotechnology Journal 19 (2021) 110–120

COMPUTATIONAL AND STRUCTURAL BIOTECHNOLOGY JOURNAL

journal homepage: www.elsevier.com/locate/csbj

Interplay of cholesterol, membrane bilayers and the AT1R: A cholesterol consensus motif on AT1R is revealed

Sofia Kiriakidi [a,c], Christos Chatzigiannis [b], Christina Papaemmanouil [b], Andreas G. Tzakos [b], Zoe Cournia [c,*], Thomas Mavromoustakos [a,*]

[a] National and Kapodistrian University of Athens, Department of Chemistry, Athens, Greece
[b] University of Ioannina, Department of Chemistry, Section of Organic Chemistry and Biochemistry, Ioannina, Greece
[c] Biomedical Research Foundation, Academy of Athens, 4 Soranou Ephessiou, 11527 Athens, Greece

ARTICLE INFO

Article history:
Received 14 September 2020
Received in revised form 21 November 2020
Accepted 23 November 2020
Available online 3 December 2020

Keywords:
Candesartan
AT1R
Cholesterol
CCM
Molecular Dynamics
DOSY
NMR
DPPC

ABSTRACT

Hypertension, mediated by the Angiotensin II receptor type 1 (AT1R), is still the major cause of premature death despite the discovery of novel therapeutics, highlighting the importance of an in depth understanding of the drug-AT1R recognition mechanisms coupled with the impact of the membrane environment on the interaction of drugs with AT1R. Herein, we examine the interplay of cholesterol-lipid-candesartan and the AT1R using Molecular Dynamics simulations of a model membrane consisting of 60:40 mol%. DPPC:cholesterol, candesartan and the AT1R, mimicking the physiological cholesterol concentration in sarcolemma membranes. The simulations of the model membrane of 60:40 mol%. DPPC:cholesterol were further validated using DOSY NMR experiments. Interestingly, our results suggest a significant role of cholesterol in the AT1R function imposed through a Cholesterol Consensus Motif (CCM) in the receptor, which could be crucial in the drug binding process. Candesartan diffusion towards AT1R through incorporation into lipid bilayers, appears to be retarded by the presence of cholesterol. However, its direct approach towards AT1R may be facilitated through the mobility induced on the N-terminus by the cholesterol binding on the CCM these novel insights could pave the way towards the development of more potent pharmaceutical agents to combat hypertension more effectively.

1. Introduction

Cardiovascular diseases (CVDs) are responsible for 31% of all deaths worldwide each year, according to recent studies by the World Health Organisation (WHO) [1,2]. Understanding of associated risk factors and promoting prevention based on a healthier lifestyle are vital population-wide strategies, while at the same time proper treatment is required for people with already established disease. Hypertension is one of the major risk factors leading to cardiovascular disease and even death if left untreated. Therefore, the benefits of lowering blood pressure for prevention of CVDs are well established [3]. Angiotensin II (AII) receptor blockers are a class of drugs used to treat hypertension by blocking the detrimental action of AII in a pathological state to act on AT1 receptor (AT1R) and propagate abnormal tension to the vessels. Candesartan is the most potent among the eight marketed drugs belonging in this class [4,5] Angiotensin II receptor type 1 (AT1R) is a G-Protein Coupled Receptor (GPCR), the ligand binding site of which is found to reside in the transmembrane domain of the receptor. In our recent study [2], we explored the candesartan/AT1R interactions and two mechanisms of drug binding; a membrane-mediated, where the drug first penetrates the lipid membrane and then laterally diffuses to the receptor's ligand binding site and a direct, where the drug tries to approach the ligand binding site through the extracellular area. Our results showed that the membrane bilayer plays an important role with respect to the candesartan-AT1R interaction, demonstrating that the neutral form of candesartan approaches the receptor by lateral diffusion through the lipid bilayer. Based on this finding, herein we study this process with a more realistic model membrane, using a binary bilayer of 60 mol.% dipalmitoyl-phosphatidyl-choline (DPPC) lipids along with 40 mol% of cholesterol, a composition that is consistent with the sarcolemma membrane [6], which is the cellular membrane where AT1R is mostly expressed [7]. Cholesterol is a sterol

* Corresponding authors.
E-mail addresses: zcournia@bioacademy.gr (Z. Cournia), tmavrom@chem.uoa.gr (T. Mavromoustakos).

https://doi.org/10.1016/j.csbj.2020.11.042
2001-0370/

lipid biosynthesized by all higher vertebrate cells and an essential structural component of the cell membrane [8]. It consists of a bulky steroid structure, which is hydroxylated at position C3, as well as a saturated hydrocarbon tail (Fig. 1).

Cholesterol has two surfaces, the "β-rough surface" in which two methyl groups attached to the quaternary carbons C18 and C19 are pointing out of the plane and the "α-smooth surface", which is defined by the lack of such methyl groups. The 3β-hydroxyl group provides amphipathicity to this lipophilic molecule and is considered as the anchor for its position in the vicinity of the lipid/water interface, while the rest of its lipophilic core resides between the hydrophobic alkyl chains of the membrane. Due to the high lipophilicity of cholesterol, it has been found that it can also occupy positions buried deep inside the membrane and close to the bilayer core, while also exhibiting a high flip-flop rate [9–14]. Moreover, cholesterol forms highly-concentrated areas, known as "lipid rafts" [15], although its solubility in the membrane is limited as it produces crystals in higher molar fractions, responsible for modifying physical properties of lipid bilayers [16]. In our recent review [17], we explored several studies indicating that the role of cholesterol as a structural component of cellular membranes is indeed vital, as it not only affects the physical properties of membranes but it also interacts with GPCRs [18,19], modifies their structure, and actively participates in the drug binding mechanism of drugs considered to act by a membrane mechanism. For example, another sartan drug that acts on AT1R, the prototype losartan, is likely to be excluded from cholesterol-rich areas, and is preferentially located in the more fluid plasma membrane regions [20,21], where it can accumulate and finally reach the AT1 receptor site. Other studies on the serotonin$_{1A}$ receptor, another important neurotransmitter of the GPCR family, showed that it exhibits cholesterol dependent functional modulation in terms of both ligand binding and G-protein coupling [22]. Further studies on this receptor indicated that there are several cholesterol "hot-spots", i.e. regions in the receptor, where cholesterol concentration is significantly denser than in other parts, both near the extracellular area and deeper in the transmembrane region [23–25]. Moreover, molecular docking studies in homology models of serotonin$_{1A}$ receptor indicated that the binding energies of all ligands (including serotonin) that were docked under this study, are stabilized in the presence of cholesterol, indicating that cholesterol facilitates the drug binding process [25]. In another example of cholesterol-GPCR functional association, Cherezov *et al* resolved two cholesterol molecules at the groove formed by *trans*-membrane (TM) helices I, II, III and IV of the β2-adrenergic receptor, and this site in the receptor crystal structure is now characterized as Cholesterol Consensus Motif (CCM) [26,27]. Further studies showed that the CCM was located on TM helix V of the β2-adrenergic receptor as a site of high cholesterol occupancy and its role as a cholesterol binding motif was confirmed [22]. Moreover, FRET studies on the haemagglutinin of influenza virus showed that a CCM is required for efficient intracellular transport and raft association of the receptor [28]. NMR studies on the peripheral-type benzodiazepine receptor also indicate a CCM which is important for the receptor's function [29]. A computational study by Guixa-Gonzalez *et al.* [30] indicated that cholesterol can even compete with orthosteric ligands by entering the receptor interior from the membrane side instead of the solvent route. Based on this literature, it is evident that cholesterol may also play a crucial role in the study of candesartan-AT1R binding, yet this role remains unknown.

Because cholesterol has been paramount in the binding of drugs associated with GPCRs, in this study we thoroughly explore the effects of cholesterol in DPPC lipid bilayers in the presence of AT1R, and compare the results with our previous study, where similar systems were investigated in the absence of cholesterol [2]. We study the neutral candesartan molecule because our previous results indicated that the anionic deprotonated form (which should be the prevalent form in physiological pH due to its very low pKa values: pKa_1 = 2.45 for the carboxyl group and pKa_2 = 6.70 for the tetrazole ring, according to SPARC, pKa/property server [32]) does not enter the lipid bilayer. Thus, we assume that in the vicinity of the membrane, candesartan becomes protonated and enters the hydrophobic lipid area. Furthermore, in this study we investigate the concentration effect of candesartan and perform additional calculations with five and ten neutral candesartan molecules in the presence of AT1R and DPPC/cholesterol bilayers. The validity of our computational studies was further confirmed by DOSY-NMR experiments using DPPC-cholesterol (60:40 mol%) vesicles in the absence of AT1R in order to measure the experimental diffusion of candesartan freely diffusing in the membrane. NMR results were compared with control MD experiments of DPPC-cholesterol (60:40 mol%) bilayers, without the AT1R, containing 26 candesartan molecules. This concentration (12.09 mol% candesartan) was used for direct comparison to the experimental concentration of 12.68 mol%.

2. Materials and methods

2.1. Materials

Candesartan cilexitil (Mw = 610.671 g/mol) was donated from CYPRIA Pharmaceutical Company and hydrolyzed to candesartan (Mw = 440.45 g/mol) by our lab according to the procedure published in Ref. [33]. DPPC (Mw = 734.039 g/mol)) was purchased

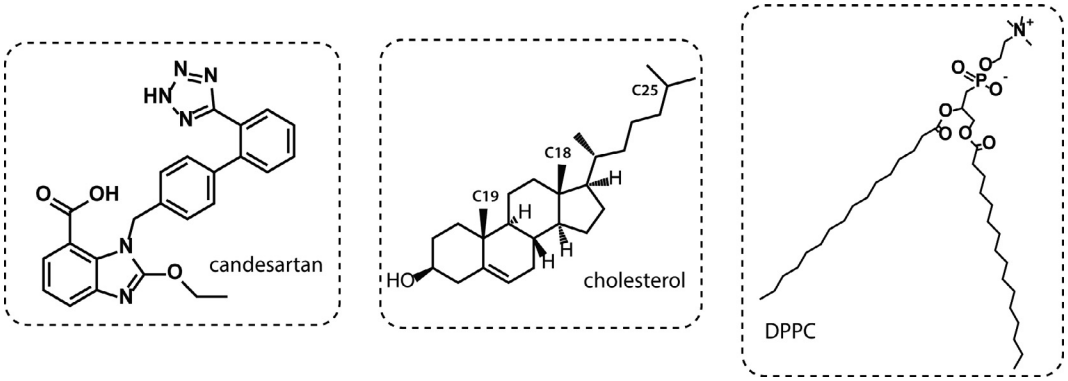

Fig. 1. 2D representation of candesartan, cholesterol, and DPPC molecules used in the molecular simulations of this study.

from AvantiPolar Lipids Inc. (Alabaster, AL) and cholesterol from Sigma Aldrich (St Louis, USA).

2.2. Methods

2.2.1. Molecular Dynamics simulations-System preparation

In the present work, three independent systems were studied with long unbiased Molecular Dynamics (MD) simulations up to 1 μs. The systems studied are presented in Fig. S1. Two additional runs for each system were conducted up to 300 ns (replica 2 and replica 3). In all systems, DPPC was the phospholipid used in the membrane bilayer, because phosphatidylcholines (PCs), especially those bearing oleic, linoleic or palmitoyl alkyl chains are the most abundant lipid species found in the plasma membranes, vascular smooth muscle cells [34] and sarcolemma cardiac membranes, while 40 mol% cholesterol was added in order to simulate the natural cholesterol percentage of the sarcolemma membranes, where AT1R is naturally expressed [35]. In all systems, the inactivated form of AT1R was used with PDB ID: 4YAY [36]. The rationale of using the inactivated and not the recently resolved active structure of the receptor [37] is thoroughly explained in our recently published study [2]. In short, according to Wingler et al. [37], who recently published the crystal structure of the activated AT1R, there is an incompatibility of the active structure with Angiotensin II receptor blockers (ARB) binding, due to orthosteric site pocket constriction in the active receptor. The BRIL apocytochrome that was used in order to facilitate crystallization was manually removed from the PDB file and any missing loops or side chains were filled in, using the homology modelling tool Prime of the Schrodinger software platform with default parameters [38]. The appropriate protonation states for the protein were assigned using Maestro's protein preparation module [39]. The first system under study (System A) consists of one neutral candesartan molecule placed in the aqueous environment over a DPPC/cholesterol lipid bilayer where AT1R is embedded. The system was hydrated with 31,602 water molecules and 256 DPPC lipids (128 on each leaflet) and 102 cholesterol molecules in a periodic box of 10.58 × 10.58 × 12.31 nm^3. Systems B and C consist of five and ten candesartan molecules, respectively, placed in the aqueous environment over a DPPC/cholesterol lipid bilayer where AT1R is embedded. All three aforementioned systems were neutralized and a 0.15 M concentration of NaCl was added in order to simulate the physiological salt concentration.

Additionally, five control systems were run fo for 300-500 ns with the same conditions, in order to test the validity of our collected data and specify the effects of the different components acting on the system. In particular, a pure DPPC, a DPPC/ATIR, a DPPC/cholesterol, a DPPC/cholesterol/AT1R and a DPPC/cholesterol/26 candesartan molecules (12.09 mol%) system were simulated. More details about the simulation times for each system are presented in Table S1.

2.2.2. Simulation protocol

All MD simulations were conducted with the computational chemistry software GROMACS 2018.1 [40]. The parameters for AT1 receptor, ions, DPPC and cholesterol molecules were described by the CHARMM36 force field [41–43], while the CHARMM36-specific TIP3P model was used for water [44]. The topology of candesartan was acquired by the SwissParam server program [45] that provides topology files in GROMACS format, based on Merck molecular force field (MMFF) [46] in a compatible form with the CHARMM36 force field. The input files were prepared using the charmm-gui interface [47]. In particular, a DPPC/cholesterol lipid bilayer with a 60:40 ratio was constructed and equilibrated. After an energy minimization using the steepest descent method with maximum 1,000,000 steps, equilibration of the system took place in the NPT ensemble. At first, an 1 ns run was conducted with position-restrains in the protein, using the V-rescale thermostat at T = 323 K and a time constant of 1 ps (in order to ensure that the lipid bilayers are in a liquid state) as well as the Berendsen barostat, with a time constant of 5 ps and compressibility of 4.5×10^{-5} bar^{-1}. Pressure was kept constant at 1 bar with semi-isotropic coupling. This short equilibration was followed by a larger equilibration run of 100 ns, using the Nosé-Hoover thermostat at T = 323 K and a time constant of 1 ps, and the Parinello-Rahman barostat with the same time constant, compressibility and pressure value as mentioned before. The convergence of the equilibration procedure is monitored through the stability of the average pressure and temperature plots presented in Fig. S2. The production runs were performed in the NPT ensemble and the equations of motion were integrated with a time step equal to 2 fs. The temperature was kept constant at 323 K using the Nosé-Hoover thermostat [48,49] with a coupling time constant equal to 1 ps. The Parrinello-Rahman barostat [50] was used in order to keep the pressure constant at 1 bar, with semiisotropic pressure coupling, with a time constant of 5 ps and compressibility of 4.5×10^{-5} bar^{-1}. Long-range electrostatics were treated with the particle mesh Ewald (PME) method. Coulomb interactions were calculated with a 1.0 nm cut-off radius and the Lennard Jones interactions were calculated using a 1.2 nm cut-off radius and the force-switch cut-off scheme. Most of the computational analyses were performed with GROMACS modules. In particular, deuterium order parameters, S_{CD}, were calculated using the gmx_order module, hydrogen bonds with gmx_hbond, distances with gmx_distance, partial densities with gmx_density, the diffusion coefficients with gmx_msd and the conformational analysis with gmx_cluster. Statistical analyses were performed with gmx analyze and excel worksheets. Error bars have been included in all relevant plots based on the three replica simulations. The averages are either replica averages or time averages, if the presented data are calculated versus time. For instance, the standard deviation included in Table 2 has been computed by averaging the hydrogen bonds over time and then averaging these data over the three replicas of each system. Error bars were computed based on the standard deviation of each set. For the S_{CD}, root mean square fluctuations, RMSF, and mean square displacements, MSD(t) plots, the error bars represent standard deviations calculated by block averaging. Additionally, the FATSLiM analysis tool [51] was used for bilayer thickness, and area per lipid calculations. VMD [52] was used for structure alignment, visualization and visual trajectory analysis.

2.2.3. Sample preparation of candesartan incorporated in DPPC/cholesterol unilamellar vesicles

Samples were prepared by dissolving 27 mg of dry DPPC with 9.54 mg cholesterol and 4.05 mg candesartan (DPPC:cholesterol ratio = 6:4 and candesartan:DPPC ratio = 1:4) in chloroform. The mixture was then evaporated at room temperature and thereafter placed under vacuum for 24 h in order to form a thin lipid film on the bottom of glass vials. The obtained mixture was further fully hydrated in 1 mL D_2O and sonicated for 15 min in Branson sonicator (4/7 power) in order to form unilamellar vesicles. The sample was then transported to a 600 μL NMR tube.

2.2.4. DOSY NMR experiments

Diffusion-ordered spectroscopy (DOSY) NMR experiments were performed using a Bruker AV 500 MHz spectrometer (Bruker Biospin, Rheinstetten, Germany), using the Topspin 2.1 suite. A pulse field gradient unit capable of producing magnetic field pulse gradients in the z-direction of 53 G cm^{-1} was used to record DOSY NMR experiments. Samples were dissolved in D_2O and then DOSY experiments were recorded. The probe temperature was adjusted to 50

°C and the samples were subjected to DOSY. The parameters utilized for acquisition time and relaxation delay were 1.09 s and 4 T_1, respectively. Afterwards, the T_1 values were determined by the inversion recovery time pulse. Specifically, T_1 values were calculated using the null point method and were proven to be in a range between 0.2 and 0.35 s for the different aromatic and aliphatic peaks. So, the T_1 value that was used for all the ^{1}H and DOSY experiments was set to an average value of 0.3 s. The DOSY experiment pulse sequence was the bipolar pulse longitudinal eddy current delay (BPPLED). Thus, 16 BPPLED spectra containing 16 K data points were collected and the eddy current delay, (Te) was set to 5 ms. Finally, the duration of the pulse field gradient, δ_g, was optimized in order to obtain 5% residual signal with the maximum gradient strength. The pulse gradient was increased using a linear from 2 to 95% of the maximum gradient strength and a linear ramp. The diffusion dimension after Fourier transformation and baseline correction were determined using the suitable option of the Topspin 2.1 suite and the Diffusion Coefficient values were calculated using the Topspin 2.1 software. Through the Analysis tab, and the T_1/T_2 relaxation option, the 2D DOSY spectrum was converted into an 1D ^{1}H spectrum. After phase and baseline correction in the 1D spectrum, a manual integration to all the peaks related was conducted. The relevant integrals were exported into relaxation mode. After the "Fitting Function" command, the "Starting Calculation" command was conducted, resulting to the calculation of the diffusion coefficient values for each peak. An average value was calculated, so the final diffusion coefficient was determined.

3. Results and discussion

3.1. Bilayer properties

Lipid bilayers can exist in several phases, among which liquid-ordered (L_o) and liquid disordered (L_d or L_α) phases are considered to be the most relevant for biological membranes [53]. Addition of cholesterol in some lipids, such as DPPC, induces the thermodynamically stable L_o phase, with characteristics in between the gel and L_d phases [54]. In this work, the deuterium order parameters for DPPC molecules, S_{CD}, were computed, which are a measure of the orientation of the C–H bonds of the hydrocarbon chains with respect to the membrane normal. Deuterium order parameters are usually expressed as the average over the angle θ between the C–H bond and the bilayer normal using the second Legendre polynomial:

$$S_{CD} = \frac{1}{2}(3 < \cos^2\theta > -1)$$

As illustrated in Fig. 2, the increase of the order parameter of the *sn1* and *sn2* DPPC chains induced by the addition of cholesterol is in agreement with experimental results, which suggest that adding cholesterol in lipid bilayers provokes the transformation from L_d to L_o phase [55].

In particular, addition of 40 mol% cholesterol to a pure DPPC bilayer increases the ordering of the bilayer significantly, inducing an average difference of 0.17 and 0.16 for the *sn1* and the *sn2* chains, respectively, with respect to the pure DPPC bilayer, while the embedding of the AT1R does not cause disordering in the pure DPPC bilayer but provokes disordering in the order of 0.02 on average, when incorporated in the DPPC-cholesterol system (Fig. 2). The incorporation of one candesartan molecule in the DPPC:cholesterol bilayer) does not show a statistically significant change in ordering, but a more pronounced disordering effect is observed when five candesartan molecules are added, with an average difference of 0.01 for both phospholipid chains. Doubling the candesartan concentration to ten molecules induces a significant increase in the disordering effect on the DPPC:cholesterol membrane with average differences of 0.09 for both phospholipid chains, indicating that there is a critical candesartan concentration above which the disordering is more pronounced. The computed order parameters for the pure DPPC bilayer and DPPC/cholesterol bilayers are in very good agreement with experimental NMR values [56–60] as shown in the comparative plot with data found in Ref. [56] and our computed data, which is presented in Fig. S3.

Another important membrane property studied in this work is the area in the cholesterol-containing membranes upon candesartan penetration. The average area occupied by a lipid molecule in the bilayer can be expressed as:

$$< A_{lipid} > = < \frac{2V_{lipid}}{h} >$$

where V_{lipid} is the volume of the lipid molecule and h is the bilayer thickness. For complex systems consisting of DPPC, cholesterol, AT1R and candesartan molecules, the membrane system is divided into polygons, using Voronoi tessellation. For each lipid, there is a corresponding Voronoi cell, the area of which is calculated and used as an approximation of the lipid accessible area. In systems where a AT1R is present, at first the calculation of the Voronoi cell is conducted as described before (i.e. as if there was no protein) and then the protein atoms are projected on the same plane as the lipids and the ones that are inside a Voronoi cell of a proximal lipid are taken into account. The center of geometry corresponding to these protein atoms is added to the Voronoi points, leading to an updated cell for the reference lipid. The area of this modified cell is then used as an approximation of the lipid's accessible area. For a more thorough description of the area per lipid and the FATSLiM analysis algorithms see ref. [51].

In this study, addition of 40 mol% cholesterol induces a reduction of 27.2% in the area per lipid as shown in Table 1, compared to the pure DPPC system, which has an area per lipid of 0.61 ± 0.01 nm^2, in very good agreement with the experimental value of 0.63 ± 0.00 nm^2 [61]. The bilayer condensation caused by cholesterol addition is in agreement with previous experimental and computational studies [54,61–65]. On the contrary, when AT1R is embedded in a pure DPPC bilayer, the area per lipid increases, as a result of the disordering effect induced to the bilayer by the protein penetration. However, when cholesterol is added to the DPPC/AT1R bilayer, the area per lipid is decreased again, indicating a consistency in the condensation that it induces. No significant increase in the area per lipid is induced when one or five candesartan molecules are embedded in the bilayer (Table 1). A disordering effect takes place inducing an increase of 0.04 nm^2 in the area per lipid, when ten candesartan molecules penetrate the DPPC:cholesterol membrane. Moreover, the bilayer thickness was also investigated. The results presented in Table 1 show that the incorporation of 40 mol% cholesterol induces an increase of 13.28% in the bilayer thickness compared to the pure DPPC bilayer, which has a thickness of 4.02 ± 0.05 nm, in very good agreement with the experimental value of 3.90 nm[61]. On the contrary, the embedded AT1R causes a reduction up to 3%, which is consistent with the disordering it induces in the bilayer. Eventually, the addition of cholesterol to the DPPC/AT1R bilayer increases the thickness by counteracting the thinning induced by AT1R, yielding a final DPPC/cholesterol/AT1R bilayer thickness of 4.65 ± 0.06 nm. Penetration of candesartan reduces the thickening induced by cholesterol, which is consistent with the disordering that it induces (Fig. 3).

Cholesterol addition in the DPPC bilayer results in a more ordered, more condensed and thicker bilayer, which exhibits a decreased fluidity compared to the pure DPPC bilayer. In contrast, the addition of one candesartan molecule causes a small disordering effect and a small increase of this effect is observed when five candesartan molecules are included. However, the addition of ten

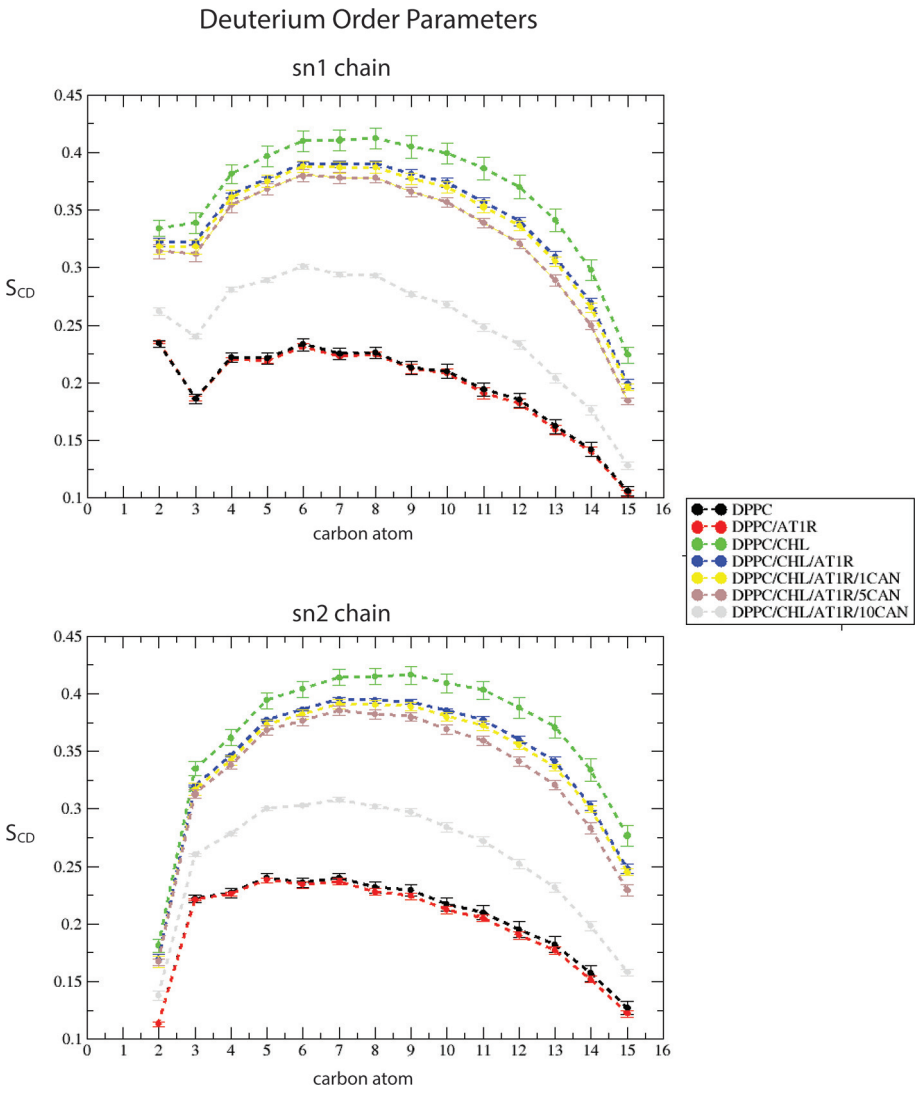

Fig. 2. MD computed deuterium order parameters for both sn1 (up) and sn2 (down) DPPC chains. The pure DPPC system is depicted in black, DPPC/AT1R in red, DPPC/cholesterol (CHL) in green, DPPC/CHL/AT1R in blue, DPPC/CHL/AT1R and one CAN molecule in yellow, DPPC/CHL/AT1R and five CAN molecules in brown and DPPC/CHL/AT1R and ten CAN molecules in silver. (For interpretation of the references to colour in this figure legend, the reader is referred to the web version of this article.)

Table 1
Average thickness and area per lipid for each system. The areas are averaged over the two leaflets.

System	Average Thickness (nm)	Area per lipid (nm^2)
DPPC	4.02 ± 0.05	0.61 ± 0.01
DPPC, AT1R	3.89 ± 0.14	0.69 ± 0.02
DPPC/CHL	4.63 ± 0.06	0.45 ± 0.01
DPPC/CHL, AT1R	4.65 ± 0.06	0.50 ± 0.01
1 CAN, DPPC/CHL, AT1R	4.62 ± 0.06	0.51 ± 0.01
5 CAN, DPPC/CHOL, AT1R	4.59 ± 0.06	0.51 ± 0.01
10 CAN, DPPC/CHL, AT1R	4.27 ± 0.04	0.55 ± 0.01

candesartan molecules results in significantly more pronounced disordering compared to the lower concentrations of candesartan. Thus, we conclude that there is a critical concentration above which, the effects of candesartan are more accented. The same trend is observed in the average bilayer thickness, where adding one or five candesartan molecule does not induce a significant change in thickness \ while the addition of ten candesartan molecules induces a more dramatic decrease to 4.27 nm ± 0.04 nm compared to 4.65 ± 0.06 nm of the DPPC:cholesterol with the embedded AT1R (Table 1). These effects result from a non-ideal mixing behaviour and are of great importance, since they indicate that the widely heterogenic cellular membranes will have a significantly different structure than ideal one-lipid type models, which may affect the functioning of transmembrane proteins [66]. A similar disordering effect was also observed for olmesartan in DPPC/cholesterol bilayers [67]. Candesartan also interacts with cholesterol molecules and provokes a 25.9 ± 14.8 degrees tilt in cholesterol orientation compared to being perpendicular (90±0.8) to the bilayer in the pure DPPC:cholesterol system, as illustrated in Fig. 3. The time evolution of cholesterol angle to the bilayer plane averaged for systems A-C is presented in Fig. S4, showing a large deviation in the tilt angles.

3.2. Cholesterol - AT1R interactions

Significant interactions of cholesterol with GPCRs have been previously reported in the literature [17,68,69]. Hence, there is a growing interest of the cholesterol role in drug binding mechanisms when GPCRs are involved.

Trajectories of 300 ns containing a pure DPPC or a 60:40 mol% DPPC/cholesterol bilayer, with AT1R embedded (control systems

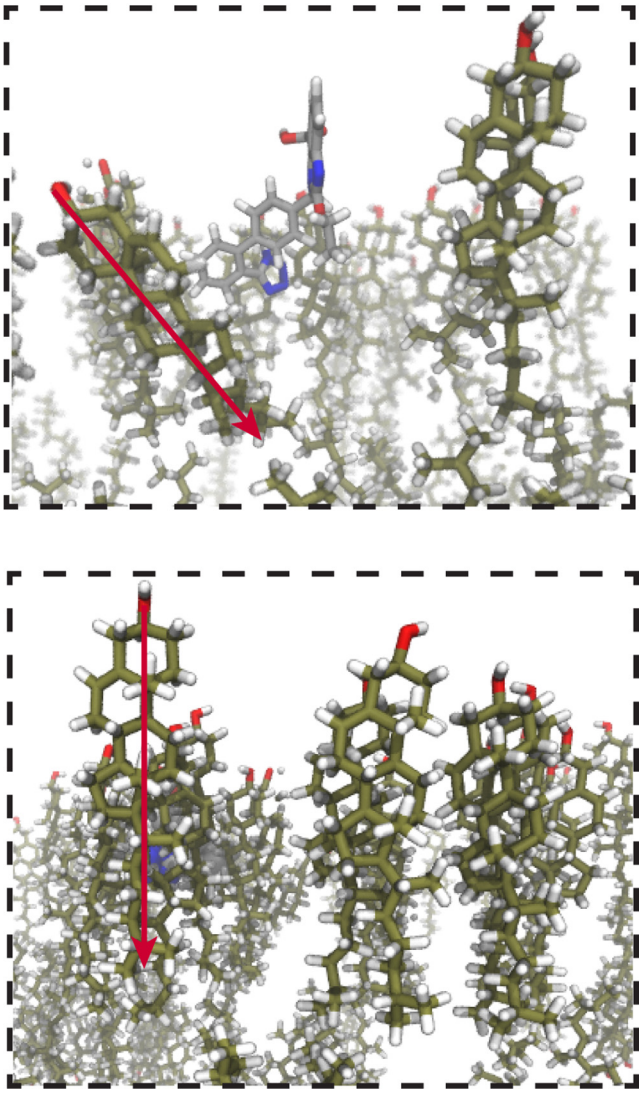

Fig. 3. Characteristic snapshots of cholesterol tilt in the proximity of candesartan (top) with respect to its vertical arrangement in the bulk membrane (bottom). The main axis vector of cholesterol (a vector connecting O and C_{23}) is depicted with a red arrow. (For interpretation of the references to colour in this figure legend, the reader is referred to the web version of this article.)

2 and 4, as presented in Table S1) were analyzed into clusters, using the gmx_cluster module and the linkage method, where a structure is added to a cluster when its distance to any element of the cluster is less than a cutoff distance set to 0.1 nm. The RMSD was calculated using the AT1R backbone atoms. The most probable cluster, i.e. the cluster containing most of the simulation frames for each of the systems was used as an input for the RMSD calculation. Thus, the average structure of AT1R, when embedded in a pure DPPC bilayer, was compared to the average structure of the receptor embedded in a 60:40 mol% DPPC/cholesterol bilayer. The RMSD of the two structures is 4.2 Å (Fig. 4). In fact, the inclusion of cholesterol in the lipid bilayer, where AT1R is embedded, induces significant structural changes with respect to the crystallographic inactivated structure. In particular, transmembrane helices VI and VII are affected the most, by being shifted 4–5 Å, as illustrated in Fig. 4-left. Moreover, as presented in Table 2, cholesterol engages in 1.16±0.9 hydrogen bonds with AT1R on average.

In all systems A-C and in all of their replicas, a cholesterol molecule is located in the hydrophobic groove formed between helices II-III-IV-V and stays there for almost all of the simulation time. Time evolution of the cholesterol carbon atom C_{25} distance from the carbon of the terminal methyl group of ILE^{151} of the putative CCM is presented in Fig. S5, while the average distances over time are presented in Table S2 and are 1.1 nm for all three simulated systems, indicating a strong and stable binding of cholesterol in this novel binding site of AT1R.

Moreover, comparative RMSF plots for AT1R embedded in a pure DPPC and in a 60:40 mol%. DPPC/cholesterol bilayer are presented in Fig. 5. It is clear that when AT1R is embedded in a cholesterol rich bilayer its overall flexibility is increased. In particular, the N-terminus (residues 1-26), which blocks the extracellular entrance to AT1R orthosteric site, is significantly more flexible and could potentially lead to a more accessible entrance. The increase in the receptor flexibility indicates a strong allosteric effect of cholesterol binding to the putative CCM. In fact, although the ordering of the bilayer induces a slower diffusion of candesartan towards the receptor through the bilayer, the flexibility induced on the receptor and in particular the mobility induced on the N-terminus may result in a more accessible extracellular entrance of candesartan to the receptor orthosteric site.

The steroid core of cholesterol rests in the non-polar environment created by residues Ile^{151} ($I^{4.53}$-according to Ballesteros-Weinstein numbering scheme), Trp^{153} ($W^{4.50}$) and Phe^{66} ($F^{2.58}$). The cholesterol hydroxyl group rests in a polar area of this groove, while it engages in hydrogen bonds with Arg^{137} of Intracellular Loop 2 (ICL2).

A schematic representation of this region is demonstrated in Fig. 4-right. The binding of cholesterol in this site is consistent with the description of CCM suggested by Hanson *et al* [27] for the class A GPCR, and might actually serve as a putative CCM for AT1R. In fact,

the CCM is an area in the TM helices of GPCRs where cholesterol binds, consisting of the following residues, according to the Ballesteros-Weinstein numbering scheme: [4.39–4.43(R,K)]—[4.50(W,Y)]—[4.46(I,V,L)]—[2.41(F,Y)]. Although not identical, the observed cholesterol binding residues serve as a similar pattern and could be suggested as a CCM for AT1R, which, to the best of our knowledge, has not yet been identified.

3.3. Candesartan localization and interactions

The computed mass densities indicate a well-structured membrane, where the cholesterol molecules lie 2 nm deep inside the DPPC bilayer, and the DPPC phosphate groups are in contact with the water interface. In System A, as illustrated in Fig. 6, the candesartan molecule is located at 1.1 ± 0.1 nm of the bilayer center, which is in agreement with our previous study [2]. Thus, the presence of cholesterol does not seem to affect the preferred candesartan localization inside the cellular membrane in spite of the significant bilayer condensation discussed previously. In cases where more than one candesartan molecules are present, such as System B with five and System C with ten molecules, respectively, all candesartan molecules enter the membrane and reside at distances from 1.1 to 1.8 nm of the bilayer center. In particular, all five molecules of system B and 8 out of 10 molecules of system C are located between 1 and 1.5 nm from the bilayer center, while two molecules are near the polar headgroups, as depicted in Fig. S6. Time-dependent distances from the bilayer center for each system averaged over 3 replicas, are illustrated in Figs. S7–S9. The average distances for each system and each candesartan molecule are presented in Table S3. Our results are in agreement with previous MD and umbrella sampling studies with the neutral form off irbesartan, which is also located at 1 nm off the bilayer center [70].

Given the complexity of the studied system, the diffusion of candesartan in the lipid bilayer was studied employing a combination of computational and experimental approaches, in order to

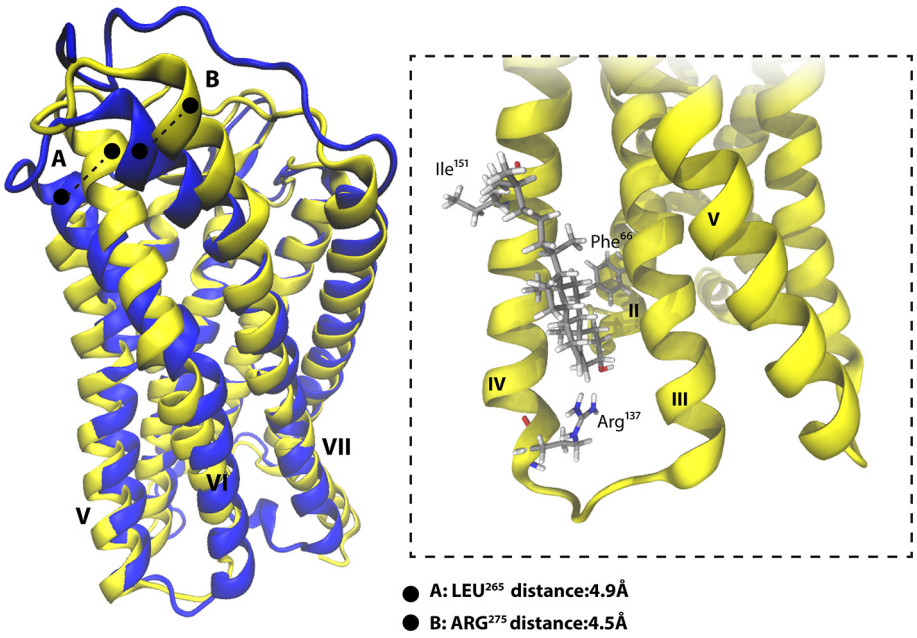

Fig. 4. AT1R after structure clustering of 300 ns MD simulation in a pure DPPC (blue) and in a mixed 60:40 DPPC:cholesterol bilayer (yellow). The transmembrane helices notation and several characteristic distances are presented (left). The RMSD of the two structures was 4.2 Å. The most deviating points are indicated with black dots: point A is a 4.9 Å tilt of TM helix VI measured at LEU^{265} and point B is a 4.5 Å tilt of TM helix VII measured at ARG^{275}. A cholesterol molecule (represented in liquorice) is resting in the hydrophobic cavity between TM helices II-III-IV-V, interacting with residues Ile^{151}, Phe^{66} and Arg^{137}, which could serve as putative CCM (right). (For interpretation of the references to colour in this figure legend, the reader is referred to the web version of this article.)

Table 2
Average number of hydrogen bonds between candesartan-AT1R, candesartan-DPPC, candesartan-cholesterol and AT1R-cholesterol for each of the simulated systems.

System	Hydrogen BONDS			
	Candesartan-protein	Candesartan-DPPC	Candesartan-cholesterol	PROTEIN-cholesterol
A	0.00 ± 0.03	0.80 ± 0.69	0.02 ± 0.12	1.58 ± 0.98
B	0.03 ± 0.03	1.18 ± 0.27	0.07 ± 0.11	0.91 ± 0.78
C	0.00 ± 0.03	1.00 ± 0.02	0.04 ± 0.07	0.98 ± 0.94

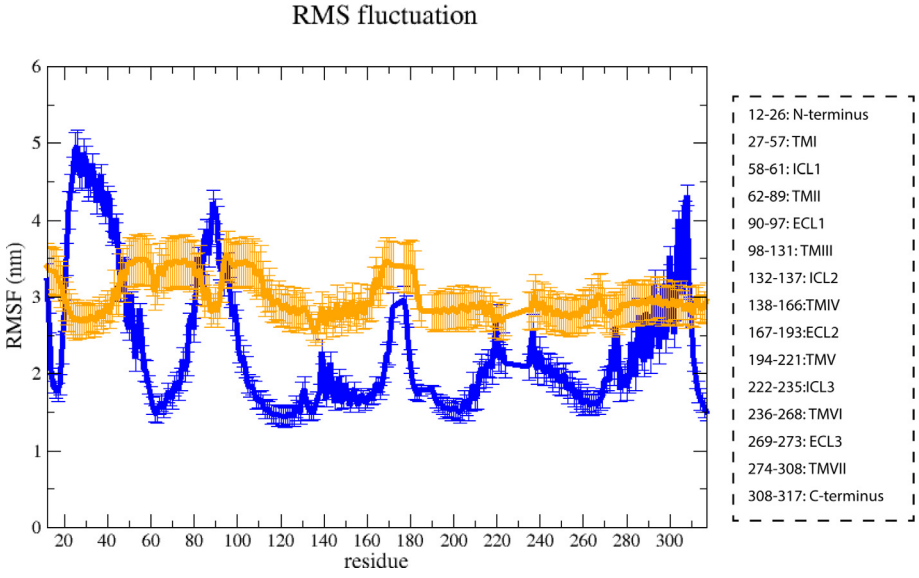

Fig. 5. RMSF plot for AT1R embedded in a pure DPPC (blue) and a 60:40 DPPC:cholesterol bilayer (orange). The legend on the right indicates the characteristic AT1R areas as per residue number. (For interpretation of the references to colour in this figure legend, the reader is referred to the web version of this article.)

confirm the validity of our model and gain further insight on the way candesartan interacts with the lipid membrane. The candesartan diffusion coefficient of 6.44 × 10^{-12} m^2/s that was calculated from DOSY NMR experiments with 60:40 DPPC/cholesterol ratio is in excellent agreement with the diffusion coefficient that was calculated computationally (9.00 ± 0.2 × 10^{-12} m^2/s) for the control

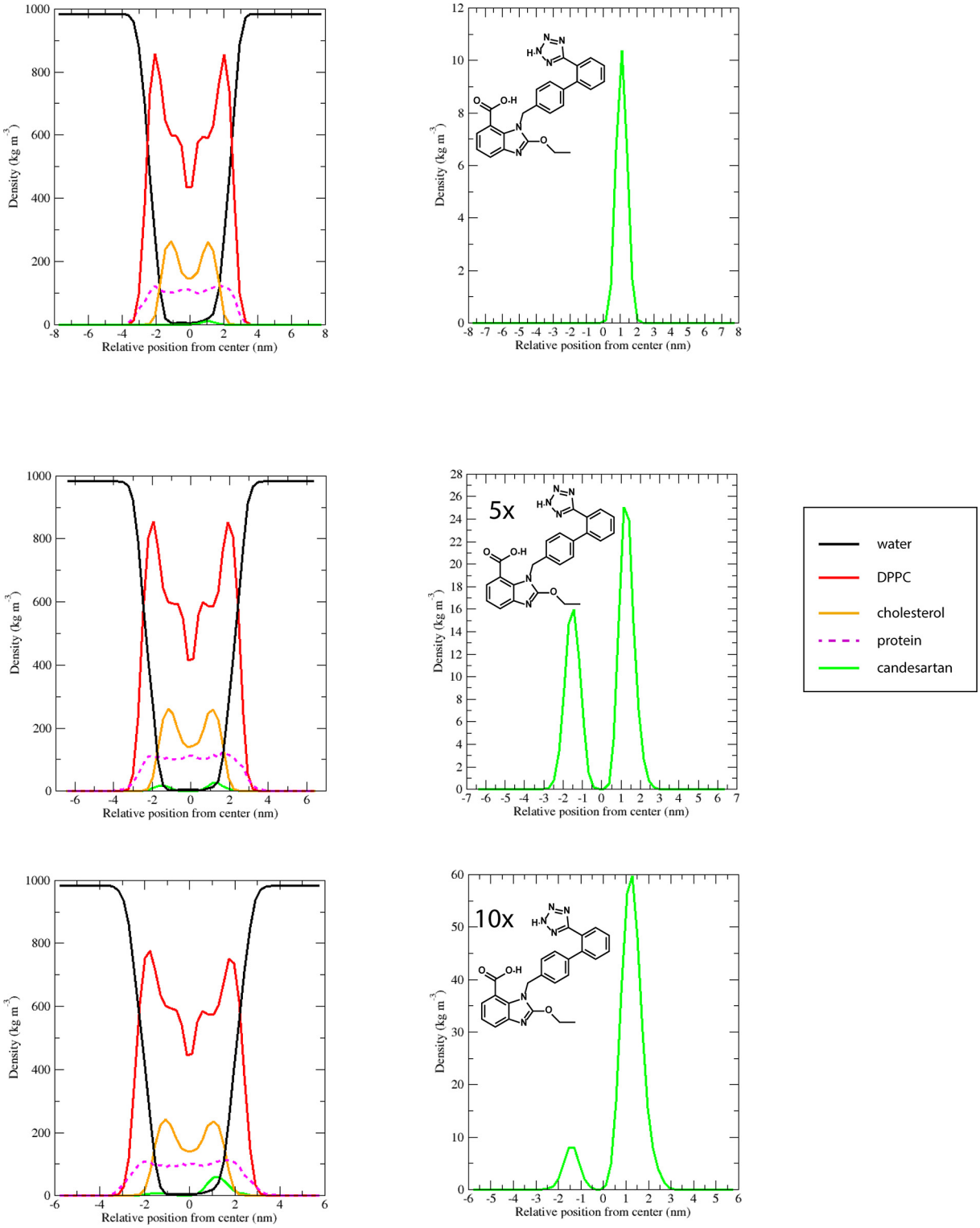

Fig. 6. Mass densities (kg/m^3) for systems A (top), B (middle) and C (bottom). The densities of CAN (green), cholesterol (orange), DPPC (red), protein (purple dashed) and water (black) are presented with respect to the corresponding moiety's relative position to the bilayer's center (left). CAN is also depicted alone for clarity (right). (For interpretation of the references to colour in this figure legend, the reader is referred to the web version of this article.)

system DPPC/cholesterol/26 candesartan molecules, i.e. 12.09 mol %. concentration. The Mean Square Deviation (MSD) plot for candesartan is presented in Fig. S10. The diffusion coefficient was calculated using the Einstein relation while fitting was performed in linear regime of the MSD(t) plot, i.e. between 75 and 250 ns as illustrated in the log–log plot of Fig. S10.

Moreover, the intermolecular interactions between candesartan, DPPC, cholesterol and AT1R were studied, by calculating the average hydrogen bonds between them and also by observing the trajectory. As presented in Table 2 and also observed throughout the trajectory video, candesartan molecules do not interact significantly with the AT1R, however, they diffuse inside the

membrane and form hydrogen bonds with the DPPC molecules. These results are in contrast with the results from our cholesterol-free simulations [2], where candesartan approaches the protein through membrane diffusion and tries to enter the orthosteric site through the transmembrane opening between the transmembrane helices IV & V. The inability of candesartan to approach the receptor through the membrane bilayer in the presence of cholesterol, although the simulation time was doubled compared to the cholesterol-free simulations (1 μs versus 500 ns), could be attributed to the fact that cholesterol enhances the bilayer ordering, induces slower diffusion of candesartan (6.44×10^{-12} in the presence of cholesterol, compared to 2.03×10^{-11} m^2/s in pure DPPC bilayers [2], as per our NMR experiments) and thus decreases the possibility of the candesartan-AT1R encounter in a given time. The slower diffusion in the more ordered, cholesterol rich bilayers is also observed by the computationally derived self-diffusion coefficients for the DPPC molecules, presented in Fig. S11. In fact, the DPPC self-diffusion coefficient in the cholesterol rich bilayers is one order of magnitude lower than in pure DPPC, indicating slower diffusion for DPPC as well.

Conformational analysis in all simulations showed that candesartan adopts two different conformations depending on its surrounding environment. The first, which is the starting conformation in all simulations, is when the benzimidazole and tetrazole rings are in opposite sides with respect to the biphenyl bond and is denoted as *trans*. The *trans* conformation is prevalent when the molecule is hydrated, but when it enters the lipid bilayer it flips to a *cis* conformation, with both the benzimidazole and tetrazole rings in the same side. The two conformations are illustrated in Fig. 7 and the results are in agreement with our previous study [2], where pure DPPC bilayers were employed, thus leading to the assumption that cholesterol does not affect the *cis/trans* conformational equilibrium.

4. Conclusions

The drug binding process to a GPCR protein is a complex procedure, depending among others on the membrane environment in which the receptor is embedded. In this study, we conducted a thorough investigation of DPPC, cholesterol, AT1R and candesartan interactions, taking into account different candesartan concentration effects in a 60:40 mol% DPPC/cholesterol bilayer. Our membrane model is validated by DOSY NMR experiments, which show a very good agreement with our computationally derived diffusion coefficients. The same applies with lipid order parameters, area per lipid and bilayer thickness, when compared to available experimental data. Cholesterol increases the ordering of the bilayer, resulting in L_o phase lipids and a more condensed bilayer. The role of cholesterol in the AT1R function is also highlighted, not only by the structural differences that it imposes on the receptor, but also by the observation of a putative CCM in the groove formed by transmembrane helices II-III-IV-V. In particular, it interacts strongly by residues Ile^{151}, Trp^{153} and Phe^{66} of TM II and TM IV for the whole simulation time of 1 μs, for all the independent simulations that were conducted. In fact, a different AT1R conformation was observed, which resulted from cholesterol interactions with the receptor and cholesterol binding in a putative CCM. This CCM could serve a novel allosteric role in affecting the flexibility of AT1R regions crucial for drug binding. The present study also

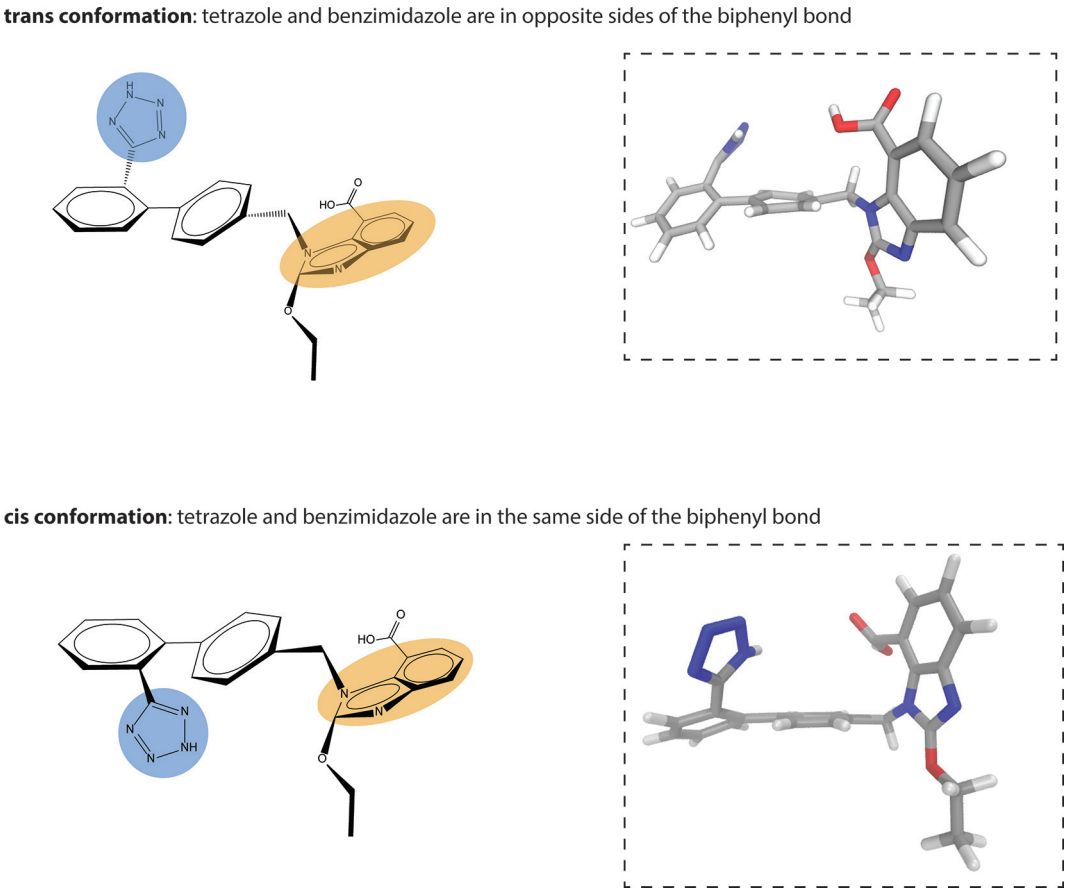

Fig. 7. Candesartan trans (top) and cis (bottom) conformation when both tetrazole and benzimidazole moieties are in the opposite or the same side of the biphenyl bond, respectively.

pinpoints that candesartan does not form any hydrogen bonds with cholesterol. Previous X-ray scattering studies [20] have shown that losartan avoids cholesterol rich areas in the bilayer. A similar behavior of candesartan could explain our findings, which show no hydrogen bonding between the two molecules. NMR and X-ray studies will be performed in the future in order to investigate this behavior in a more detailed fashion. Additionally, further studies are needed to validate experimentally the novel indication that was observed in this work, i.e. the CCM on AT1R, which could serve a significant role in the drug binding process.

Moreover, additional computational studies comparing the kinetics of the direct and indirect binding mechanisms will shed light upon the most probable binding pathway. As shown in the present study, the more ordered bilayer provokes a slower membrane diffusion for candesartan, which may favor the direct instead of the indirect membrane-mediated, drug binding mechanism. The understanding of the AT1R:drug binding mechanism can lead to the design of much more potent drugs treating hypertension, one of the most widespread diseases of our times.

Acknowledgement

This research work was supported by the Hellenic Foundation for Research and Innovation (HFRI) and the General Secretariat for Research and Technology (GSRT), under the HFRI PhD Fellowship grant (GA. no. 14551) awarded to SK. The molecular dynamics simulations of this research work were supported by computational time granted from the Greek Research & Technology Network (GRNET) in the National HPC facility—ARIS—under project ID AT1R and project number pr007008_thin- and from the DECI-15 HPC facility—under project ID 15DECI0334 AT1R. Materials were supported by Special Account for Research Grants (SARG), National Kapodistrian University of Athens (NKUA). Preliminary NMR experiments, before establishing the final conditions, were supported by CERIC 20187056. This research work was also supported by the Hellenic Foundation for Research and Innovation (H.F.R.I.) under the "First Call for H.F.R.I. Research Projects to support Faculty members and Researchers and the procurement of high-cost research equipment grant" (Project Number: 1780) awarded to ZC.

Appendix A. Supplementary data

Supplementary data to this article can be found online at https://doi.org/10.1016/j.csbj.2020.11.042.

References

[1] Mendis S, Puska P, Norrving Bo, editors. Global Atlas on Cardiovascular Disease Prevention and Control. Geneva: World Health Organization; 2011.
[2] Kiriakidi S, Chatzigiannis C, Papaemmanouil C, Tzakos AG, Mavromoustakos T. Exploring the role of the membrane bilayer in the recognition of candesartan by its GPCR AT1 receptor. Biochim Biophys Acta BBA 2020;1862:183142.
[3] Ettehad D, Emdin CA, Kiran A, Anderson SG, Callender T, Emberson J, et al. Blood pressure lowering for prevention of cardiovascular disease and death: a systematic review and meta-analysis. Lancet 2016;387:957–67.
[4] Unger T. Pharmacological aspects of candesartan, an effective AT1-receptor blocker. Eur Heart J Suppl 2004;6:h11–6.
[5] Wagenaar LJ, Voors AA, Buikema H, van Buiten A, Lübeck RH, Boonstra PW, et al. Functional antagonism of different angiotensin II Type I Receptor Blockers In Human Arteries. Cardiovasc Drugs Ther 2002;16:311–6.
[6] Fiehn W, Peter JB, Mead JF, Gan-Elepano M, Lipids and fatty acids of sarcolemma, sarcoplasmic reticulum, and mitochondria from rat skeletal muscle, J Biol Chem, 246, (1971), 5617–5620.
[7] Powers SK, Morton AB, Hyatt H, Hinkley MJ. The renin-angiotensin system and skeletal muscle. Exerc Sport Sci Rev 2018;46:205–14.
[8] Grouleff J, Irudayam SJ, Skeby KK, Schiøtt B. The influence of cholesterol on membrane protein structure, function, and dynamics studied by molecular dynamics simulations. Biochim Biophys Acta BBA 2015;1848:1783–95.
[9] Genheden S, Essex JW, Lee AG. G protein coupled receptor interactions with cholesterol deep in the membrane. Biochim Biophys Acta BBA 2017;1859:268–81.
[10] Harroun TA, Katsaras J, Wassall SR. Cholesterol hydroxyl group is found to reside in the center of a polyunsaturated lipid membrane. Biochemistry 2006;45:1227–33.
[11] Kučerka N, Perlmutter JD, Pan J, Tristram-Nagle S, Katsaras J, Sachs JN. The effect of cholesterol on short- and long-chain monounsaturated lipid bilayers as determined by molecular dynamics simulations and X-ray scattering. Biophys J 2008;95:2792–805.
[12] Bennett WFD, MacCallum JL, Hinner MJ, Marrink SJ, Tieleman DP. Molecular view of cholesterol flip-flop and chemical potential in different membrane environments. J Am Chem Soc 2009;131:12714–20.
[13] Javanainen M, Martinez-Seara H. Rapid diffusion of cholesterol along polyunsaturated membranes via deep dives. Phys Chem Chem Phys 2019;21:11660–9.
[14] Pinkwart K, Schneider F, Lukoseviciute M, Sauka-Spengler T, Lyman E, Eggeling C, et al. Nanoscale dynamics of cholesterol in the cell membrane. J Biol Chem 2019;294:12599–609.
[15] Korade Z, Kenworthy AK. Lipid rafts, cholesterol, and the brain. Neuropharmacology 2008;55:1265–73.
[16] Wassall SR, Stillwell W. Polyunsaturated fatty acid–cholesterol interactions: Domain formation in membranes. Biochim Biophys Acta BBA 2009;1788:24–32.
[17] Kiriakidi S, Kolocouris A, Liapakis G, Ikram S, Durdagi S, Mavromoustakos T. Effects of cholesterol on GPCR function: insights from computational and experimental studies. In: Rosenhouse-Dantsker A, Bukiya A, editors. In: Rosenhouse-Dantsker A., Bukiya A. (eds), Direct Mechanisms in Cholesterol Modulation of Protein Function advances in experimental medicine and biology. Cham: Springer; 2019. p. 89–103. 1135.
[18] Bista RK, Bruch RF, Covington AM. Variable-temperature Raman spectromicroscopy for a comprehensive analysis of the conformational order in PEGylated lipids. J Raman Spectrosc 2009;40:463–71.
[19] Deganutti G, Moro S. Estimation of kinetic and thermodynamic ligand-binding parameters using computational strategies. Future Med Chem 2017;9:507–23.
[20] Hodzic A, Zoumpoulakis P, Pabst G, Mavromoustakos T, Rappolt M. Losartan's affinity to fluid bilayers modulates lipid–cholesterol interactions. Phys Chem Chem Phys 2012;14:4780–8.
[21] Kellici FT, Tzakos GA, Mavromoustakos T. Rational drug design and synthesis of molecules targeting the angiotensin II type 1 and type 2 receptors. Molecules 2015;20:3868–97.
[22] Sengupta D, Prasanna X, Mohole M, Chattopadhyay A. Exploring GPCR–lipid interactions by molecular dynamics simulations: excitements, challenges, and the way forward. J Phys Chem B 2018;122:5727–37.
[23] Sengupta D, Chattopadhyay A. Identification of cholesterol binding sites in the serotonin1A receptor. J Phys Chem B 2012;116:12991–6.
[24] Sengupta D, Chattopadhyay A. Molecular dynamics simulations of GPCR–cholesterol interaction: An emerging paradigm. Biochim Biophys Acta BBA 2015;1848:1775–82.
[25] Paila Y, Tiwari S, Sengupta D, Chattopadhyay A. Molecular modeling of the human serotonin1A receptor: role of membrane cholesterol in ligand binding of the receptor. Mol BioSyst 2010;7:224–34.
[26] Cherezov V, Rosenbaum DM, Hanson MA, Rasmussen SGF, Thian FS, Kobilka TS, et al. High-resolution crystal structure of an engineered human β₂-adrenergic g protein-coupled receptor. Science 2007;318:1258–65.
[27] Hanson MA, Cherezov V, Griffith MT, Roth CB, Jaakola VP, Chien EYT, et al. A specific cholesterol binding site is established by the 2.8 Å structure of the human beta2-adrenergic receptor. Structure 2008;16:897–905.
[28] de Vries M, Herrmann A, Veit M. A cholesterol consensus motif is required for efficient intracellular transport and raft association of a group 2 HA from influenza virus. Biochem J 2015;465:305–14.
[29] Jamin NG, Neumann J-M, Ostuni MA, Vu TKN, Yao Z-X, Murail S, et al. Characterization of the cholesterol recognition amino acid consensus sequence of the peripheral-type benzodiazepine receptor. Mol Endocrinol 2005;19:588–94.
[30] Guixà-González R, Albasanz JL, Rodriguez-Espigares I, Pastor M, Sanz F, Martí-Solano M, et al. Membrane cholesterol access into a G-protein-coupled receptor. Nat Commun 2017;8:14505.
[32] Hilal S, Karickhoff S, Carreira L. Prediction of the Solubility, Activity Coefficient and Liquid/Liquid Partition Coefficient of Organic Compounds. QSAR Comb. Sci. 2004;23:709–20.
[33] Ntountaniotis D, Kellici T, Gkeka P, Cournia Z, Galdadas I, Mali G, et al. Drug-membrane interactions in the renin angiotensin system: applications and practical considerations. In: Demetzos C, Pippa N, editors. Thermodynamics and Biophysics of Biomedical Nanosystems. Singapore: Springer; 2019. p. 339–64.
[34] Oliveira TR, Lamy MT, De Paula UM, Guimarães LL, Toledo MS, Takahashi HK, et al. Structural properties of lipid reconstructs and lipid composition of normotensive and hypertensive rat vascular smooth muscle cell membranes. Braz J Med Biol Res 2009;42:844–53.
[35] Netticadan TJ, Ashavaid TF, Nair KG. Characterisation of the canine cardiac sarcolemma in experimental myocardial ischemia. Indian J Clin Biochem 1997;12:49–54.
[36] Zhang H, Unal H, Gati C, Han GW, Liu W, Zatsepin N, et al. Structure of the Angiotensin Receptor Revealed by Serial Femtosecond Crystallography. Cell 2015;161:833–44.
[37] Wingler LM, McMahon C, Staus DP, Lefkowitz RJ, Kruse AC. Distinctive activation mechanism for angiotensin receptor revealed by a synthetic nanobody. Cell 2019;176:479–490.e12.

[38] Bell JA, Cao Y, Gunn JR, Day T, Gallicchio E, Zhou Z, et al. *PrimeX* and the Schrödinger computational chemistry suite of programs. In: Brock CP, Hahn T, Wondratschek H, Müller U, Shmueli U, Prince E, et al., editors. In: International Tables for Crystallography. Volume F: Crystallography of biological macromolecules.. Wiley; 2012. p. 534–8.
[39] Maestro, editor New York : SchrödingerSchrödinger Release; 2020-2. p. 2020.
[40] Berendsen HJC, van der Spoel D, van Drunen R. GROMACS: A message-passing parallel molecular dynamics implementation. Comput Phys Commun 1995;91:43–56.
[41] Best RB, Zhu X, Shim J, Lopes PEM, Mittal J, Feig M, et al. Optimization of the additive CHARMM all-atom protein force field targeting improved sampling of the backbone φ, ψ and side-chain χ(1) and χ(2) dihedral angles. J Chem Theory Comput 2012;8:3257–73.
[42] Klauda JB, Venable RM, Freites JA, O'Connor JW, Tobias DJ, Mondragon-Ramirez C, et al. Update of the CHARMM all-atom additive force field for lipids: validation on six lipid types. J Phys Chem B 2010;114:7830–43.
[43] Venable RM, Luo Y, Gawrisch K, Roux B, Pastor RW. Simulations of anionic lipid membranes: development of interaction-specific ion parameters and validation using NMR data. J Phys Chem B 2013;117:10183–92.
[44] Mark P, Nilsson L. Structure and dynamics of the TIP3P, SPC, and SPC/E water models at 298 K. J Phys Chem A 2001;105:9954–60.
[45] Zoete V, Cuendet MA, Grosdidier A, Michielin O. SwissParam: A fast force field generation tool for small organic molecules. J Comput Chem 2011;32:2359–68.
[46] Halgren TA. Merck molecular force field. I. Basis, form, scope, parameterization, and performance of MMFF94. J Comput Chem 1996;17:490–519.
[47] Jo S, Cheng X, Lee J, Kim S, Park S-J, Patel DS, et al. CHARMM-GUI 10 years for biomolecular modeling and simulation. J Comput Chem 2017;38:1114–24.
[48] Hoover WG. Canonical dynamics: equilibrium phase-space distributions. Phys Rev A 1985;31:1695–7.
[49] Nosé S. A molecular dynamics method for simulations in the canonical ensemble. Mol Phys 1984;52:255–68.
[50] Parrinello M, Rahman A. Polymorphic transitions in single crystals: A new molecular dynamics method. J Appl Phys 1981;52:7182–90.
[51] Buchoux S. FATSLiM: a fast and robust software to analyze MD simulations of membranes. Bioinformatics 2017;33:133–4.
[52] Humphrey W, Dalke A, Schulten K. VMD - Visual molecular dynamics. Mol Graph 1996;14:33–8.
[53] Vermeer LS, de Groot BL, Réat V, Milon A, Czaplicki J. Acyl chain order parameter profiles in phospholipid bilayers: computation from molecular dynamics simulations and comparison with 2H NMR experiments. Eur Biophys J 2007;36:919–31.
[54] Wang Y, Gkeka P, Fuchs JE, Liedl KR, Cournia Z. DPPC-cholesterol phase diagram using coarse-grained molecular dynamics simulations. Biochim Biophys Acta BBA 2016;1858:2846–57.
[55] Vist MR, Davis JH. Phase equilibria of cholesterol/dipalmitoylphosphatidylcholine mixtures: deuterium nuclear magnetic resonance and differential scanning calorimetry. Biochemistry 1990;29:451–64.
[56] Douliez JP, Léonard A, Dufourc EJ. Restatement of order parameters in biomembranes: calculation of C-C bond order parameters from C-D quadrupolar splittings. Biophys J 1995;68:1727–39.
[57] Petrache HI, Dodd SW, Brown MF. Area per lipid and acyl length distributions in fluid phosphatidylcholines determined by 2H NMR spectroscopy. Biophys J 2000;79:3172–92.
[58] Clarke JA, Seddon JM, Law RV. Cholesterol containing model membranes studied by multinuclear solid state NMR spectroscopy. Soft Matter 2009;5:369–78.
[59] Mannock DA, Lee MYT, Lewis RNAH, McElhaney RN. Comparative calorimetric and spectroscopic studies of the effects of cholesterol and epicholesterol on the thermotropic phase behaviour of dipalmitoylphosphatidylcholine bilayer membranes. Biochim Biophys Acta BBA 2008;1778:2191–202.
[60] Urbina JA, Pekerar S, Le H-B, Patterson J, Montez B, Oldfield E. Molecular order and dynamics of phosphatidylcholine bilayer membranes in the presence of cholesterol, ergosterol and lanosterol: a comparative study using 2H-, 13C- and 31P-NMR spectroscopy. Biochim Biophys Acta BBA 1995;1238:163–76.
[61] Kucerka N, Nagle JF, Sachs JN, Feller SE, Pencer J, Jackson A, et al. Lipid bilayer structure determined by the simultaneous analysis of neutron and X-ray scattering data. Biophys J 2008;95:2356–67.
[62] Berkowitz ML, Bostick DL, Pandit S. Aqueous solutions next to phospholipid membrane surfaces: insights from simulations. Chem Rev 2006;106:1527–39.
[63] Cournia Z, Ullmann GM, Smith JC. Differential effects of cholesterol, ergosterol and lanosterol on a dipalmitoyl phosphatidylcholine membrane: A Molecular Dynamics Simulation Study. J Phys Chem B 2007;111:1786–801.
[64] Edholm O, Nagle JF. Areas of molecules in membranes consisting of mixtures. Biophys J 2005;89:1827–32.
[65] Marsh D. Liquid-ordered phases induced by cholesterol: A compendium of binary phase diagrams. Biochim Biophys Acta BBA 2010;1798:688–99.
[66] de Meyer F, Smit B. Effect of cholesterol on the structure of a phospholipid bilayer. Proc Natl Acad Sci USA 2009;106:3654–8.
[67] Ntountaniotis D, Mali G, Grdadolnik SG, Maria H, Skaltsounis A-L, Potamitis C, et al. Thermal, dynamic and structural properties of drug AT1 antagonist olmesartan in lipid bilayers. Biochim Biophys Acta BBA 2011;1808:2995–3006.
[68] Fantini J, Di Scala C, Baier CJ, Barrantes FJ. Molecular mechanisms of protein-cholesterol interactions in plasma membranes: Functional distinction between topological (tilted) and consensus (CARC/CRAC) domains. Chem Phys Lipids 2016;199:52–60.
[69] Gimpl G. Interaction of G protein coupled receptors and cholesterol. Chem Phys Lipids 2016;199:61–73.
[70] Liossi AS, Ntountaniotis D, Kellici TF, Chatziathanasiadou MV, Megariotis G, Mania M, et al. Exploring the interactions of irbesartan and irbesartan–2-hydroxypropyl-β-cyclodextrin complex with model membranes. Biochim Biophys Acta BBA 2017;1859:1089–98.